

**Atomic Structure of Light-Induced Efficiency-Degrading  
Defect in Boron-doped Czochralski Silicon Solar Cells**

Journal:	<i>Energy &amp; Environmental Science</i>
Manuscript ID	EE-ART-06-2021-001788.R1
Article Type:	Paper
Date Submitted by the Author:	02-Aug-2021
Complete List of Authors:	Meyer, Abigail; Colorado School of Mines, Chemical Engineering; National Renewable Energy Laboratory, Taylor, Craig; Colorado School of Mines, Physics Venuti, Michael; Colorado School of Mines, Physics Eley, Serena; Colorado School of Mines, Physics LaSalvia, Vincenzo; National Renewable Energy Laboratory, Nemeth, William; National Renewable Energy Laboratory Page, Matthew; National Renewable Energy Laboratory Young, David; National Renewable Energy Laboratory, Stradins, Paul; National Renewable Energy Laboratory, Agarwal, Sumit; Colorado School of Mines, Chemical Engineering

## ARTICLE

## Atomic Structure of Light-Induced Efficiency-Degrading Defect in Boron-doped Czochralski Silicon Solar Cells

Abigail R. Meyer,<sup>a,c</sup> P. Craig Taylor,<sup>b</sup> Michael B. Venuti,<sup>b</sup> Serena Eley,<sup>b</sup> Vincenzo LaSalvia,<sup>c</sup> William Nemeth,<sup>c</sup> Matthew Page,<sup>c</sup> David L. Young,<sup>c</sup> Paul Stradins,<sup>\*c</sup> and Sumit Agarwal<sup>a,c</sup>

Received 00th June 20xx,  
Accepted 00th June 20xx

DOI: 10.1039/x0xx00000x

Boron-doped Czochralski (Cz) Si is the most commonly used semiconductor in the fabrication of solar cells. The minority carrier lifetime in boron-doped Cz Si decreases upon light exposure due to B-O related defects and thus, reduces performance of  $\sim 10^9$  solar modules worldwide. Using electron paramagnetic resonance (EPR), we have identified spin-active paramagnetic signatures of this phenomenon and gained insights into its microscopic mechanism. We found a distinct defect signature, which diminishes when the degraded sample is annealed. The second signature, a broad magnetic field spectrum, due to unionized B acceptors, is present in the annealed state but vanishes upon light exposure. These observations show that on degradation nearly all the  $\sim 10^{16}$  cm<sup>-3</sup> B atoms in Cz Si are complexed with interstitial O atoms, but only  $\sim 10^{12}$  cm<sup>-3</sup> of these complexes create defects that are recombination-active. The formation rate of these recombination-active defects that correlates with the decay of the minority carrier lifetime. The line shape parameters tie this defect to both B and O impurities in Cz Si.

### Introduction

Performance degradation in photovoltaic devices during normal operation is ubiquitous.<sup>1</sup> In Si-based solar cells, which represent  $\sim 96\%$  of the solar market, creation of performance-degrading defects is particularly important as the economically useful lifetimes of these devices can approach 40 years.<sup>2</sup> Boron-doped Czochralski (Cz) Si, which contains  $\sim 10^{16}$  and  $\sim 10^{18}$  cm<sup>-3</sup> substitutional B atoms and interstitial O atoms, respectively,<sup>3</sup> is the most widely used semiconductor material for fabricating solar cells.<sup>4, 5</sup> The passivated emitter rear contact (PERC) cell fabricated from boron-doped Cz Si currently accounts for  $\sim 80\%$  of the c-Si solar cells manufactured (see Figure 1a). It has been known for almost 50 years that upon injection of excess charge carriers, either via light or a forward-bias voltage, a recombination-active defect with a density of  $\sim 10^{12}$ – $10^{13}$  cm<sup>-3</sup>, is formed in B-doped Cz Si solar cells. This phenomenon, referred to as light-induced degradation (LID), is thought to be caused by a B-O complex.<sup>6</sup> These recombination-active defects in Cz Si are formed gradually, lowering the minority carrier lifetime and the solar cell's efficiency by  $\sim 2\%$  relative to the initial value.<sup>6</sup> Upon annealing in the dark at  $\sim 200$  °C, this defect becomes non-recombination-active, but this annealed state is metastable and can be reversed to the degraded state upon light exposure.<sup>7,8</sup> More recently, it has been empirically shown

that after injection of H into the bulk, annealing the degraded B-doped Cz Si under illumination at  $\sim 150$ – $180$  °C renders this defect permanently recombination-inactive (see Figure 1b).<sup>9</sup> This state is stable under further light exposure, and is referred to as the regenerated state. As most of the characterization of these three states has been based on minority carrier lifetime spectroscopy,<sup>10</sup> the atomic-level structure of the degraded, annealed, and regenerated states remains elusive. Without an atomic level understanding of LID and especially regeneration of B-doped Cz Si, it is not possible to predict the stability of the regenerated state over the 30–40 year lifespan of solar cells, which has implications on tens of gigawatts of *p*-type PERC cells that will be deployed worldwide yearly over the next decade. The LID defect concentration in B-doped Cz Si is proportional to the product of the B concentration and the square of the O concentration.<sup>6</sup> Accordingly, the light-induced degraded state in B-doped Cz Si is attributed to a complex consisting of a substitutional B atom and an interstitial O dimer.<sup>6</sup> Deep-level transient spectroscopy shows that the trap density in B-doped Cz Si after LID is  $\sim 10^{12}$ – $10^{13}$  cm<sup>-3</sup>, which makes it difficult to determine the structure of these defects with most spectroscopic tools. In this Article we show using low-temperature electron paramagnetic resonance (EPR) and magnetic susceptibility measurements that concomitant defects are formed during LID involving the B acceptors at densities several orders of magnitude greater (at least  $10^{16}$  cm<sup>-3</sup>) than those affecting the minority carrier lifetimes. In addition, both these defects involving the B acceptors, and the magnetic susceptibility measurements show the sample is diamagnetic at low temperatures implying that these defects possess an effective negative electron-electron correlation energy (negative *U*). An EPR signal related to the recombination-active

<sup>a</sup> Department of Chemical and Biological Engineering, Colorado School of Mines, Golden, CO, USA, 80401.

<sup>b</sup> Department of Physics, Colorado School of Mines, Golden, CO, USA, 80401.

<sup>c</sup> National Renewable Energy Laboratory, Golden, CO, USA, 80401.

† Electronic Supplementary Information (ESI) available: [Experimental results that further support the claims found in this paper but are not required to prove these claims]. See DOI: 10.1039/x0xx00000x

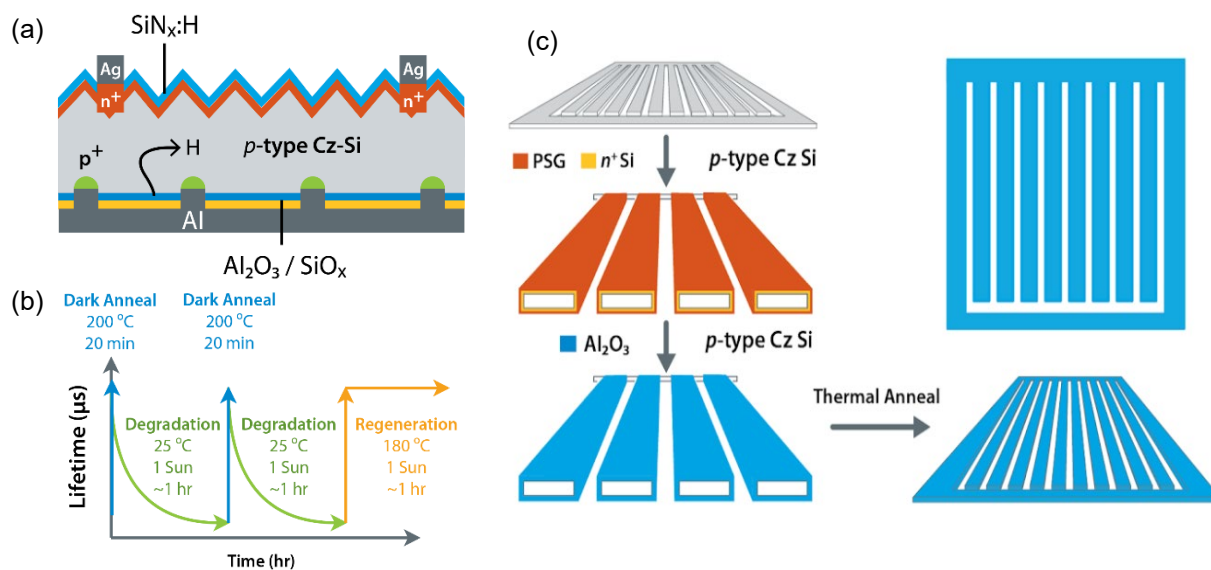


**Figure 1** (a) Schematic of the boron-doped Cz Si passivated emitter rear contact (*p*-PERC) cell, with photoconversion efficiency approaching ~24%. Currently, these cells represent the leading solar cell technology, and this trend is expected to continue for another decade. The factory efficiency of commercially-produced these solar cells does not reflect the efficiency in the field over the lifetime of the panels due to performance degradation. (b) Schematic representation of the minority carrier lifetime change in boron-doped Cz Si in the light-induced degraded, annealed, and regenerated states. Hydrogen injected from the dielectric passivation layers shown in (a) is required to obtain the regenerated state. (c) Schematic of sample preparation for EPR measurements in the “degraded” and “annealed” states. Up to six 2×20 mm<sup>2</sup> Si pieces were inserted into the quartz tube holder with a sample volume of ~0.01 cm<sup>3</sup>.

defects on the order of 10<sup>12</sup>–10<sup>13</sup> cm<sup>-3</sup> was also observed with line shape parameters that tie it to both B and O impurities in Cz Si, and a formation rate that correlates with the decay of the minority carrier lifetime.

## Results and Discussion

### Transition from Paramagnetic to Diamagnetic in Broad EPR Magnetic Scans

Figure 2a shows the EPR intensity over a broad magnetic field range (~0–800 mT) for B-doped Cz Si in the annealed, partially degraded, fully degraded, and regenerated states, and after light exposure of the regeneration state. A B-doped FZ sample, which is expected not to undergo LID due to the low interstitial O concentration (~10<sup>16</sup> cm<sup>-3</sup>), was used as reference. This sample was dark-annealed at the same conditions as the Cz Si wafers, followed by 5 min of indoor light exposure. The three states of LID — annealed, fully degraded, and regenerated — have distinctly different broad EPR spectra. In the annealed state of LID, EPR spectra show broad signatures due to the presence of frozen-out holes on B atoms.<sup>11</sup> This EPR signature of un-ionized B acceptors in Si under high mechanical stress was first observed in 1960 by Feher *et al.*<sup>12</sup> and more recently in less stressed samples by several other authors<sup>11, 13, 14</sup> (see Figure S.1 for a comparison of the literature and our experimental data on EPR spectra of B acceptors). The EPR signal in the broad magnetic field range, which extends past the range of the EPR spectrometer, is due to the fine structure term of the spin Hamiltonian, since the B acceptor has a nuclear spin of *S* = 3/2. Surprisingly, the broad B acceptor signatures disappear after 5 min of indoor light exposure at room temperature (see Figure

2a), and the sample becomes diamagnetic, but this change from a paramagnetic to a diamagnetic state does not occur if the sample is subjected to light exposure at 6 K. We suggest that the decline in the broad EPR signal after light exposure at room temperature comes about due to an interaction between B and O atoms in the Si bulk where the holes typically associated with the B acceptor are captured at a shallow, spin-less trap state nearby the B atom (Figure. 2b). This trapping results in the transition from a paramagnetic signal in the annealed state to a diamagnetic signal in the degraded state. This transition from paramagnetic to diamagnetic behavior after the first few minutes of light exposure is consistent with the fast recombination center (FRC) reported in the literature during the early state of LID,<sup>15</sup> and with a defect that has negative-*U* properties, as recently proposed.<sup>10, 16</sup> Since this initial degraded state captures almost all the holes at 6 K, it suggests that the early stage of LID is associated with a light-induced shallow hole trap, which is deeper than the B ionization energy, and is spinless. This change accounts for ~10<sup>16</sup> cm<sup>-3</sup> B atoms in Si bulk. Only a small fraction of these interactions between B and O atoms create the defect center that causes LID, which has a defect density of ~10<sup>12</sup> cm<sup>-3</sup>. Thus, we hypothesize that a small fraction of the previously passivated B acceptors is re-activated in the form of a shallow, spin-active hole trap as the sample transitions from the metastable annealed state to the degraded state. After the EPR sample is regenerated, the broad EPR spectrum returns (see Figure 2a), but not nearly to the same intensity as that of the annealed state, and is relatively featureless. In the regenerated state, no further change in the broad magnetic field spectrum was observed after 1 Sun

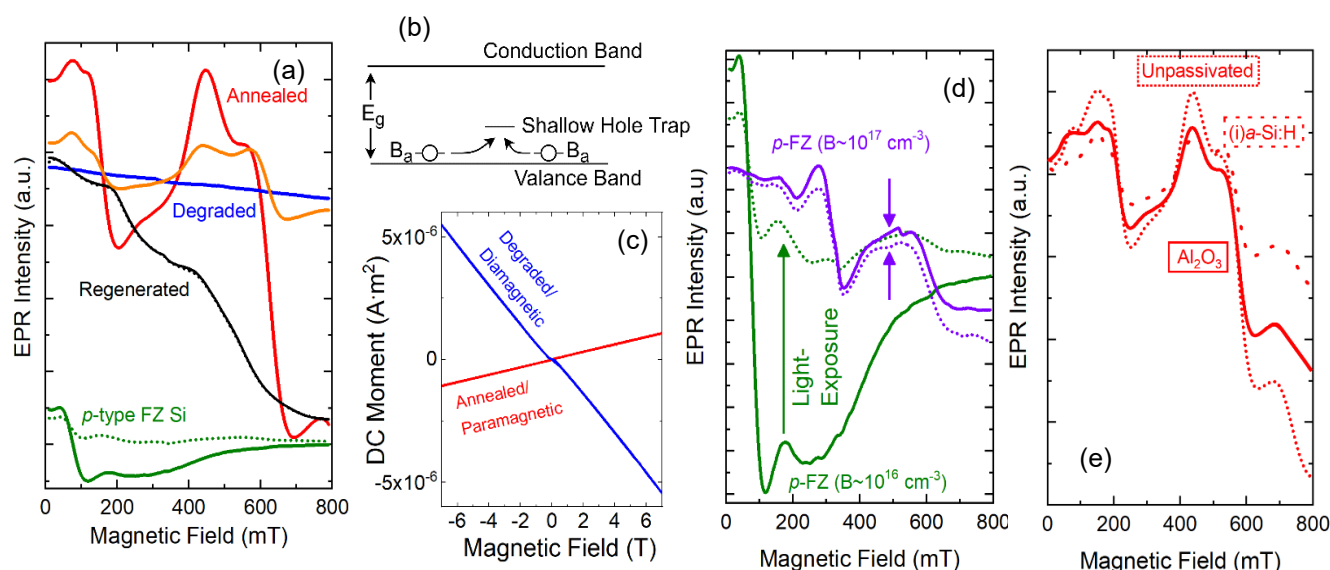


**Figure 2** (a) EPR spectra recorded over a wide range of magnetic field in B-doped Cz Si in the annealed (—), partially degraded (—), fully degraded (—), and regenerated (—) states. The EPR spectrum after illumination of the regenerated sample (---) is almost unchanged. Spectra for B-doped FZ Si after dark annealing (—) and after light-exposure (---) of the annealed sample are shown as reference. All EPR spectra were recorded at a temperature of 6 K. (b) Shallow trap state representing the early stages of LID which is likely associated with the creation of a negative-U, spinless, shallow trap involving a B atom and an oxygen dimer. (c) Magnetic susceptibility measurements of *p*-Cz Si samples in the dark annealed (—) and degraded (—) states of LID. The annealed state of LID is paramagnetic, and the degraded state of LID is diamagnetic. (d) Broad magnetic field EPR spectra of boron acceptors in *p*-FZ Si ( $[O] \lesssim 10^{16} \text{ cm}^{-3}$ ) with  $[B] \sim 10^{16}$  (—) and  $\sim 10^{17}$  (---)  $\text{cm}^{-3}$ . The dashed lines are samples exposed to ambient light for 5 min. For  $[B]:[O] \sim 1$ ,  $\sim 1/3$  of the original, dark-annealed EPR spectrum remains. When  $[B]:[O] \sim 10$ , there is minimal decline in the EPR broad spectrum intensity after light-exposure. The EPR signal intensity in Figures 2a, 2d and 2e is extremely complex due to sample to sample variations. Thus changes in the signals and not the absolute intensity units are important in interpreting these spectra. (e) Broad magnetic field EPR spectrum of boron acceptors with no passivation (---), and after surface passivation with intrinsic amorphous hydrogenated Si (---) and  $\text{Al}_2\text{O}_3$  (—). Thus, the EPR signal in the broad magnetic spectra at 6 K is due to boron acceptors in the Si lattice and is not due to surface phenomena.

illumination for 60 min (see Figure 2a), which is consistent with the stability of the regenerated state under light exposure.

To reveal the transition from the paramagnetic to diamagnetic state upon light exposure, we used DC magnetometry (Quantum Design MPMS3) on B-doped Cz Si samples in the annealed and degraded states. Figure 3 shows the DC magnetic moment as a function of magnetic field for B-doped Cz Si after dark annealing and indoor light exposure for 30 min. The slope of the line in Figure 2c provides the magnetic susceptibility: if the sample is paramagnetic, the slope is positive and if the sample is diamagnetic, the slope is negative. The magnetic susceptibility measurements in Figure 2c are consistent with the interpretation of the EPR spectra in Figure 2a, and confirm that the B-doped Cz Si in the annealed state of LID is paramagnetic, and transitions to a diamagnetic state upon indoor light exposure at room temperature.

In Figure 2a, the EPR spectrum of B-doped FZ Si also shows broad signatures due to the presence of frozen-out B acceptors,<sup>11</sup> but their intensity and line shape are different from B-doped Cz Si due to the different strain fields.<sup>13</sup> With a lower concentration of oxygen ( $\sim 10^{16}$ ), the B-doped FZ sample does not undergo LID to the same degree and thus, in contrast to the B-doped Cz sample, remains paramagnetic: this is apparent in Figure 2a from the broad EPR spectrum after light exposure which still shows the same features, but at a lower intensity. Therefore, when the oxygen content in the sample is reduced by nearly two orders of magnitude, the quenching of the B spins

is reduced. Thus, the transition from paramagnetic to diamagnetic behavior in the B-doped Cz Si samples requires both B and O atoms, further supporting the hypothesis that this transition is related to the B-O defect responsible for LID, but involves several orders of magnitude more sites, likely associated with oxygen. Any future theoretical models<sup>10, 17-19</sup> of LID defects will need to be consistent with this paramagnetic to diamagnetic transition. Figure 2d shows a comparison of the degree of spin quenching in two FZ samples with different boron concentrations,  $[B]$ , of  $\sim 10^{16}$  and  $10^{17} \text{ cm}^{-3}$ . The oxygen concentration,  $[O]$ , in FZ Si is  $\sim 10^{16} \text{ cm}^{-3}$ . In the broad EPR spectra in Figures 2a and 2d, the intensity of the broad EPR signal should not be interpreted from the absolute scale on the y-axis but from the difference of the maxima and minima in each spectrum. Therefore, in Figures 2a and 2d the spectra with lower variation in intensity indicate that the EPR signal due to the frozen out B acceptors has been partially or completely quenched. In the FZ Si sample where  $[B] > [O]$ , we observe less spin quenching than when  $[B] \sim [O]$  in FZ Si (see Figure 2d). This confirms that the paramagnetic to diamagnetic transition is related to the B-O complex. As expected, *n*-type, phosphorus-doped Cz Si does not exhibit a broad EPR signal, and does not degrade upon indoor light exposure (see Figure S.2). Finally, we performed broad magnetic field EPR scans for samples with no passivation and for those passivated with  $\text{Al}_2\text{O}_3$  and intrinsic amorphous Si (see Figure 2e). Since these spectra are very

similar, this confirms that this broad EPR signature is a bulk and not a surface phenomenon.

#### Correlating Narrow EPR Spectra to Minority Carrier Lifetime Measurements

The narrow-range (approximately 15 mT) EPR spectra in Figure 3a show signal from a distinct defect at much lower densities that directly corresponds to the LID defects in the degraded, annealed, partially degraded, and regenerated states. The broader features in Figure 3a, which results in a non-flat baseline, are due mostly to the large amount of un-ionized B acceptors in the annealed state and a small number of un-ionized B acceptors that remain after LID and regeneration, as discussed above. After the sample was exposed to light for 24 hr, a strong, narrow EPR signal appears at  $\sim 335$  mT, corresponding to  $g = 2.003 \pm 0.0005$ . This 24 hr timescale of increase in intensity of the EPR signature of the B-O LID defect is consistent with the slow recombination center (SRC) reported in the literature.<sup>15</sup> In comparison, the EPR spectrum of the annealed state of LID is almost featureless at  $\sim 335$  mT. This signal disappears after annealing but reappears upon exposure to indoor light ( $\sim 10^{-2}$  Suns) for  $\sim 30$  min, albeit at a reduced intensity indicating a partially-induced LID state. Finally, when the sample is regenerated, the EPR signal at  $\sim 335$  mT permanently disappears, and the spectrum is relatively featureless. We confirm that the sample is indeed in the regenerated state as the EPR spectrum remains unchanged after subsequent exposure to 1 Sun illumination for 1 hr. We confirmed that this EPR signature at  $\sim 335$  mT does not appear

in phosphorus-doped Cz Si or boron-doped FZ Si (see Figure S.3). Furthermore, this narrow EPR defect signature correlates with the minority photocarrier lifetime curves shown in Figure 3b. As expected, the lifetimes are almost identical in the annealed and regenerated states, and the lifetime does not change after light exposure of the regenerated sample. Additionally, we fitted the lifetime curve in the fully degraded state in Figure 3b assuming Shockley-Reed-Hall recombination at a single trap site, and Auger recombination as the primary mechanisms.<sup>20</sup> The expression used to model the surface contribution was based on Krügener *et al.*<sup>21</sup> The fitted parameters include the capture cross section ratio,  $k$ , the saturation current density,  $J_0$ , and trap density,  $N_t$ . The fitted parameters yield an electron-to-hole capture cross section ratio of  $\sim 10$ , which is consistent with the ratio for the B-O LID defect reported in the literature.<sup>22</sup> These observations further confirm that the EPR signature at a  $g$ -value of  $\sim 2.003 \pm 0.0005$  is related to the B-O LID defect. We also conducted narrow magnetic field EPR scans on the annealed and light-exposed  $p$ -FZ and  $n$ -Cz Si samples and do not observe the EPR defect signature at  $\sim 335$  mT. Finally, the inverse minority carrier lifetime, which is proportional the defect density, has a linear relationship to the EPR peak-to-peak amplitude, providing strong evidence that the defect detected in EPR is responsible for the LID (see Figure 3c). The EPR peak-to-peak amplitude, or intensity, is calculated by subtracting the maximum point from the minimum point of the EPR signature in the vicinity of  $\sim 335$  mT in Figure 3a. The non-zero  $y$ -axis intercept indicates that the sample has a finite initial lifetime due to other defects even when the LID defect is not active.

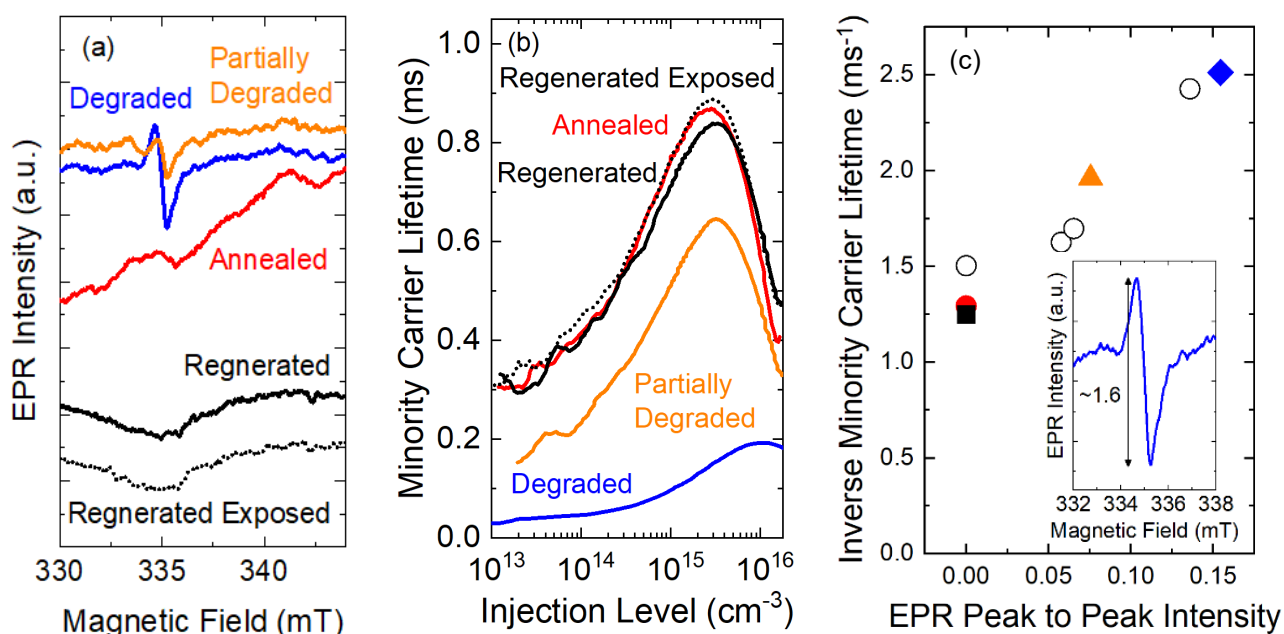


**Figure 3** (a) Narrow range EPR spectra for B-doped Cz Si, in the annealed (—), partially degraded (—), fully degraded (—), regenerated (—) states of the B-O complex, and after light exposure of the regenerated (---) state. After the sample goes through regeneration or subsequent light-exposure, no EPR signature at  $g$ -value  $\sim 2.003$  appears. (b) Minority carrier lifetime curves for each of the samples in (a) with the same color notation. (c) Inverse minority carrier lifetime of B-doped Cz Si sample at  $10^{15}$  cm<sup>-3</sup> injection level, plotted as a function of peak to peak amplitude of narrow magnetic field EPR signature in the annealed (●), partially degraded (▲), fully degraded (◆), regenerated (■) states of LID, and after various degradation times (○). The symbol sizes used approximately represent the lifetime measurement accuracy of 3%. Inset: narrow range EPR signal due to LID defects in  $p$ -Cz Si, in the fully degraded (—) state.

The inset in Figure 3c shows the EPR spectrum for a *p*-type Cz Si sample in the fully degraded state of LID over a narrower, 6 mT, magnetic field range. The peak-to-peak intensity of the EPR signature at 335 mT is  $\sim 1.6$  intensity units in the fully degraded state of LID. The absolute number of spins,  $N_s$ , is related to the peak-to-peak intensity,  $S_{EPR}$  as

$$S_{EPR} = A \cdot \left(\frac{N_s}{T}\right) \cdot \sqrt{P} \cdot V_{sample} \cdot M \quad (1)$$

where  $S_{EPR}$  is the EPR signal detected,  $A$  is a characteristic factor that depends on the instrument,  $N_s$  is the absolute number of spins,  $T$  is sample temperature,  $P$  is the microwave power,  $V_{sample}$  is the volume of sample, and  $M$  is the modulation amplitude. The signal from the Cz Si sample is calibrated with a weak pitch sample where the number of spins is known in a defined sample volume. This comparison yields a spin density of  $2 \times 10^{12} \pm 1 \times 10^{12} \text{ cm}^{-3}$  in the fully degraded state, which is consistent with DLTS measurements.<sup>23</sup> The line shape of the EPR spectrum with its Gaussian wings and peak-to-peak width of approximately 1 mT indicates that the linewidth is likely determined by different orientations of the B-O complex and random inhomogeneities in the vicinity of the defect sites. The spectrum is also anisotropic since the low field positive component is somewhat broader and shorter than the high field negative component. In addition, we did not find any significant angular dependence of the EPR signal (at 0, 45, and 90° EPR sample rotation), which is also consistent with random inhomogeneities as the dominant factor contributing to the line shape (see Figure S.4).

The EPR signal at  $g = 2.003$  is closer to the free electron value (2.0023) than typical defects only residing on a Si atom, such as that of a Si dangling bond with  $g$ -value of 2.0055. This observation suggests that oxygen atoms are involved in the wavefunction of the unpaired spin, similar to the  $P_b$  centers, where the  $g$ -value decreases as the number of oxygen atoms involved increases<sup>24, 25</sup> and  $E'$  centers in  $\text{SiO}_2$  (see Table S.1 for a summary of other spin-active defects commonly found in *c*-Si).<sup>26</sup> This trend suggests that a fraction of the wave function of this defect is on two or more oxygen atoms, which is consistent with earlier models for the B-O LID defect<sup>6, 10</sup> that involve an oxygen dimer.

## Conclusions

In summary, we have shown that the light-induced degradation in B-doped Cz Si results in a distinct EPR signature of an associated defect with  $g=2.003$ , at densities  $\sim 10^{12}$ – $10^{13} \text{ cm}^{-3}$ . Surprisingly, the early-stage LID also causes massive changes in the EPR spectra of  $\sim 10^{16} \text{ cm}^{-3}$  frozen-out B acceptors and a transition from a paramagnetic to a diamagnetic state. This effect is likely associated with the creation of a negative-U shallow trap involving a B atom and an oxygen dimer in the Cz Si. Besides studying LID, the highly-sensitive magnetic resonance tools and sample preparation techniques developed in this study can be extended to reveal other types of performance degrading defects in Cz Si and other

semiconductor materials used in photovoltaics including CdTe and perovskites.

## Experimental Procedures

As-sawn, 180- $\mu\text{m}$ -thick, boron- ( $[\text{B}] \sim 10^{16} \text{ cm}^{-3}$ ) and phosphorus-doped ( $[\text{P}] \sim 1.5 \times 10^{15} \text{ cm}^{-3}$ ) Czochralski (Cz) Si wafers, and 280- $\mu\text{m}$ -thick boron-doped ( $[\text{B}] \sim 10^{16} \text{ cm}^{-3}$ ) Float Zone (FZ) Si wafers were laser scribed into 30 $\times$ 50 mm<sup>2</sup> tokens along with a “comb-like” structure towards the center (see Figure 1(c)). Each “tooth” of the comb structure was 2 $\times$ 20 mm<sup>2</sup> to ensure that it can fit into the quartz sample tube of the electron paramagnetic resonance (EPR) spectrometer. In addition to samples for EPR, sister samples were scribed into 30 $\times$ 50 mm<sup>2</sup> tokens, but without the comb structure. These samples underwent identical processing steps, and were used for measuring the minority carrier lifetime with a Sinton lifetime tester (WCT-120). After laser scribing, the samples were subjected to a saw-damage removal process using 22.5% KOH at 70 °C for 15 min. The samples were then cleaned with a standard piranha and RCA process prior to  $\text{POCl}_3$  gettering at 785 °C for 30 min to getter impurities to the surface. The resulting phosphosilicate glass and the phosphorous-doped layer were etched off in HF and KOH solutions, respectively. After this, the samples were recleaned. All surfaces of samples that were studied in EPR in their degraded and dark-annealed states were passivated with  $\sim 15 \text{ nm}$  thick  $\text{Al}_2\text{O}_3$  deposited via atomic layer deposition (ALD) using  $\text{Al}(\text{CH}_3)_3$  and  $\text{H}_2\text{O}$  at 150 °C. After ALD, the samples were annealed in forming gas at 400 °C for 20 min. In these tokens, the defect states responsible for light-induced degradation (LID) were created under 1-Sun illumination at room temperature for 24 hr. The defect states in partially degraded samples were created under ambient light at an intensity of  $\sim 10^{-2}$  Sun. After LID, the samples were dark-annealed at 200 °C for 20 min to create the non-recombination-active, metastable “annealed” state. Before the EPR measurements, each tooth in the Si token was snapped, leaving only a 1 mm wide top edge that was not passivated with  $\text{Al}_2\text{O}_3$ . The exceptional surface passivation with  $\text{Al}_2\text{O}_3$  minimized the spin-active Si dangling bonds on the surface.

In Si tokens where the carrier lifetime was regenerated after LID, the  $\text{Al}_2\text{O}_3$  layer had to be removed in a 10% HF solution. After this, on both sides of each Si token, a  $\sim 70\text{-nm}$ -thick, H-rich  $\text{SiN}_x$  film was deposited.  $\text{SiN}_x$  dielectric layers ( $n \sim 2$ ) were plasma-deposited using  $\text{SiH}_4$  (2 sccm) and  $\text{NH}_3$  (24 sccm) at 0.4 Torr pressure, at a substrate temperature of 350 °C, and 24 mW/cm<sup>2</sup> radio-frequency (rf) power density at 13.56 MHz. After  $\text{SiN}_x$  deposition, the Si tokens were fired in a furnace to inject hydrogen incorporated into  $\text{SiN}_x$  into bulk *c*-Si, which is necessary for regeneration from LID. During fast-firing, the ramp up, dwell, and ramp down steps were each 15 s with a peak temperature calibrated to  $\sim 800$  °C. The  $\text{SiN}_x$  film was subsequently etched in 10% HF, and both sides of the token were passivated with a plasma-deposited intrinsic amorphous hydrogenated Si (*i/a*-Si:H) film. The symmetric passivating 20 nm *i/a*-Si:H layers were plasma deposited on the samples using  $\text{SiH}_4$  (10 sccm) and  $\text{H}_2$  (60 sccm) at 0.5 Torr pressure, 250 °C

## ARTICLE

## Energy &amp; Environmental Science

substrate temperature, and 12 mW/cm<sup>2</sup> rf power density at 13.56 MHz. The symmetric passivating *i/a*-Si:H layers were chosen instead of Al<sub>2</sub>O<sub>3</sub> grown by ALD as Al<sub>2</sub>O<sub>3</sub> passivation of the *c*-Si surface requires annealing in forming gas at 400 °C to activate the surface passivation. We found that this activation annealing step likely results in a redistribution of the hydrogen injected in bulk *c*-Si from SiN<sub>x</sub> making it impossible for the minority carrier lifetime in the sample to be regenerated.<sup>8</sup> After surface passivation with *i/a*-Si:H, to convert the samples to the non-recombination-active “regenerated” state, they were exposed to 1 Sun illumination at 175 °C for 2 hr. After regeneration, similar to the samples in the “degraded” and the “annealed” states, several toothbrushes were snapped off for the EPR measurements.

EPR measurements were performed at 6 K, ~0.6 mW microwave power, and 3 G modulation amplitude. Up to six 2×20 mm<sup>2</sup> Si pieces were inserted into the quartz tube holder with a sample volume of ~0.01 cm<sup>3</sup>. Our EPR instrument has a sensitivity of ~10<sup>10</sup> spins. Therefore, our measurements are sensitive to a spin-active defect density of ~10<sup>12</sup> cm<sup>-3</sup>. For magnetic susceptibility measurements, the 2×20 mm<sup>2</sup> Si pieces were further cleaved into ~2×2 mm<sup>2</sup> pieces and the data was recorded at 6 K over a range of -7 to 7 T.

### Author Contributions

**Abigail R. Meyer** – Data curation, conceptualization, funding acquisition, formal analysis, investigation, methodology, resources, visualization, writing – original draft and review and editing

**P. Craig Taylor** – Conceptualization, methodology, supervision, writing – original draft and review and editing

**Michael B. Venuti** – Investigation

**Serena Eley** – Investigation, resources

**Vincenzo LaSalvia** – Methodology

**William Nemeth** – Methodology

**Matthew Page** – Methodology

**David L. Young** – Supervision, project administration

**Paul Stradins** – Methodology, supervision, project administration, conceptualization, funding acquisition, methodology, validation, writing – original draft and review and editing

**Sumit Agarwal** – Methodology, supervision, project administration, conceptualization, funding acquisition, validation, writing – original draft and review and editing

### Conflicts of interest

“There are no conflicts to declare”.

### Acknowledgements

Funding for this work was provided by the US DOE EERE contracts SETP DE-EE0008984 and SETP DE-EE0008171 and under Contract No. DE-AC36-08GO28308. The publisher, by accepting the article for publication, acknowledges that the U.S. Government retains a nonexclusive, paid up, irrevocable, worldwide license to publish or reproduce the published form of this work, or allow other to do so, for U.S. Government purposes. This work was authored in part by the National Renewable Energy Laboratory, operated by Alliance for Sustainable Energy, LLC, for the U.S. Department of Energy (DOE) under Contract No. DE-AC36-08GO28308. Funding provided by the U.S. Department of Energy Office of Energy Efficiency and Renewable Energy Solar Energy Technologies Office. The views expressed in the article do not necessarily represent the views of the DOE or the U.S. Government. The U.S. Government retains and the publisher, by accepting the article for publication, acknowledges that the U.S. Government retains a nonexclusive, paid-up, irrevocable, worldwide license to publish or reproduce the published form of this work, or allow others to do so, for U.S. Government purposes.

### References

- 1 Queisser, H. J.; Haller, E. E., Defects in semiconductors: Some fatal, some vital. *Science* 1998, 281 (5379), 945-950.
- 2 Hallam, B.; Herguth, A.; Hamer, P.; Nampalli, N.; Wilking, S.; Abbott, M.; Wenham, S.; Hahn, G., Eliminating Light-Induced Degradation in Commercial p-Type Czochralski Silicon Solar Cells. *Appl. Sci.-Basel* 2018, 8 (1), 19.
- 3 Borghesi, A.; Pivac, B.; Sassella, A.; Stella, A., Oxygen Precipitation in Silicon. *J. Appl. Phys.* 1995, 77 (9), 4169-4244.
- 4 Green, M. A., The Passivated Emitter and Rear Cell (PERC): From conception to mass production. *Sol. Energy Mater. Sol. Cells* 2015, 143, 190-197.
- 5 International Technology Roadmap for Photovoltaic (ITRPV); 1492; April 2020.
- 6 Bothe, K.; Schmidt, J., Electronically activated boron-oxygen-related recombination centers in crystalline silicon. *J. Appl. Phys.* 2006, 99 (1), 11.
- 7 Wilking, S.; Herguth, A.; Hahn, G., Influence of hydrogen on the regeneration of boron-oxygen related defects in crystalline silicon. *J. Appl. Phys.* 2013, 113 (19), 6.
- 8 Wilking, S.; Beckh, C.; Ebert, S.; Herguth, A.; Hahn, G., Influence of bound hydrogen states on BO-regeneration kinetics and consequences for high-speed regeneration processes. *Sol. Energy Mater. Sol. Cells* 2014, 131, 2-8.
- 9 Nampalli, N.; Li, H. Z.; Kim, M.; Stefani, B.; Wenham, S.; Hallam, B.; Abbott, M., Multiple pathways for permanent deactivation of boron-oxygen defects in p-type silicon. *Sol. Energy Mater. Sol. Cells* 2017, 173, 12-17.
- 10 Markevich, V. P.; Vaqueiro-Contreras, M.; De Guzman, J. T.; Coutinho, J.; Santos, P.; Crowe, I. F.; Halsall, M. P.; Hawkins, I.; Lastovskii, S. B.; Murin, L. I.; Peaker, A. R., Boron-Oxygen Complex Responsible for Light-Induced Degradation in Silicon Photovoltaic Cells: A New Insight into the Problem. *Phys. Status Solidi A-Appl. Mat.* 2019, 216 (17), 10.
- 11 Neubrand, H., ESR from Boron in Silicon at Zero and Small External Stress. 2. Linewidth and Crystal Defects. *Phys. Status Solidi B-Basic Res.* 1978, 90 (1), 301-308.

- 12 Feher, G.; Hensel, J. C.; Gere, E. A., Paramagnetic Resonance Absorption from Acceptors in Silicon. *Phys. Rev. Lett.* 1960, 5 (7), 309-311.
- 13 Neubrand, H., ESR from Boron in Silicon at Zero and Small External Stress. 1. Line Positions and Line Structure. *Phys. Status Solidi B-Basic Res.* 1978, 86 (1), 269-275.
- 14 Tezuka, H.; Stegner, A. R.; Tyryshkin, A. M.; Shankar, S.; Thewalt, M. L. W.; Lyon, S. A.; Itoh, K. M.; Brandt, M. S., Electron paramagnetic resonance of boron acceptors in isotopically purified silicon. *Phys. Rev. B* 2010, 81 (16).
- 15 Niewelt, T.; Schon, J.; Warta, W.; Glunz, S. W.; Schubert, M. C., Degradation of Crystalline Silicon Due to Boron-Oxygen Defects. *IEEE J. Photovolt.* 2017, 7 (1), 383-398.
- 16 Vaquero-Contreras, M.; Markevich, V. P.; Coutinho, J.; Santos, P.; Crowe, I. F.; Halsall, M. P.; Hawkins, I.; Lastovskii, S. B.; Murin, L. I.; Peaker, A. R., Identification of the mechanism responsible for the boron oxygen light induced degradation in silicon photovoltaic cells. *J. Appl. Phys.* 2019, 125 (18), 16.
- 17 Schmidt, J.; Bothe, K., Structure and transformation of the metastable boron- and oxygen-related defect center in crystalline silicon. *Phys. Rev. B* 2004, 69 (2), 8.
- 18 Voronkov, V. V.; Falster, R.; Bothe, K.; Lim, B., Light-induced lifetime degradation in boron-doped Czochralski silicon: are oxygen dimers involved? *Proceedings of the 3rd International Conference on Crystalline Silicon Photovoltaics (Siliconpv 2013)* 2013, 38, 636-641.
- 19 Voronkov, V. V.; Falster, R.; Bothe, K.; Lim, B.; Schmidt, J., Lifetime-degrading boron-oxygen centres in p-type and n-type compensated silicon. *J. Appl. Phys.* 2011, 110 (6), 7.
- 20 Rahman, M. Z.; Khan, S. I., Advances in surface passivation of c-Si solar cells. *Materials for Renewable and Sustainable Energy* 2012, 1, 1.
- 21 Krugener, J.; Haase, F.; Rienacker, M.; Brendel, R.; Osten, H. J.; Peibst, R., Improvement of the SRH bulk lifetime upon formation of n-type POLO junctions for 25% efficient Si solar cells. *Sol. Energy Mater. Sol. Cells* 2017, 173, 85-91.
- 22 Lindroos, J.; Savin, H., Review of light-induced degradation in crystalline silicon solar cells. *Sol. Energy Mater. Sol. Cells* 2016, 147, 115-126.
- 23 McHedlidze, T.; Weber, J., Direct detection of carrier traps in Si solar cells after light-induced degradation. *Phys. Status Solidi-Rapid Res. Lett.* 2015, 9 (2), 108-110.
- 24 Lang, V.; Murphy, J. D.; Falster, R. J.; Morton, J. J. L., Spin-dependent recombination in Czochralski silicon containing oxide precipitates. *J. Appl. Phys.* 2012, 111 (1), 7.
- 25 Koizuka, M.; Yamada-Kaneta, H., Electron spin resonance centers associated with oxygen precipitates in Czochralski silicon crystals. *J. Appl. Phys.* 2000, 88 (4), 1784-1787.
- 26 Buscarino, G.; Agnello, S.; Gelardi, F. M.,  $(^{29}\text{Si})$  hyperfine structure of the  $E'_{\alpha}$  center in amorphous silicon dioxide. *Phys. Rev. Lett.* 2006, 97 (13), 4.